Project information

Project full title	European network for developing new horizons for RIs
Project acronym	EURIZON
Grant agreement no.	871072
Instrument	Research and Innovation Action (RIA)
Duration	01/02/2020 – 31/01/2024
Website	https://www.eurizon-project.eu/

Deliverable information

Deliverable no.	D3.10
Deliverable title	Publication of results on VCN transmission through novel VCN moderator materials
Deliverable responsible	V.V. Nesvizhevsky
Related Work-Package/Task	WP3
Type (e.g. Report; other)	Publications
Author(s)	V.V. Nesvizhevsky
Author(s) affiliation	Institut Max von Laue – Paul Langevin, Grenoble, France
Dissemination level	Public
Document Version	1.2
Date	20.02.2024
Download page	

Document information

Version no.	Date	Author(s)	Comment
1.0	19.02.2024	V.V. Nesvizhevsky	
1.1	20.02.2024	V.V. Nesvizhevsky	Reviewed by S. Mattauch
1.2	21.02.2024	V.V. Nesvizhevsky	Reviewed by J. Marauska

This project has received funding from the European Union's Horizon 2020 research and innovation programme under grant agreement No. 871072.

Overview of the publications

Title	Date	Author(s)	Comment
Effect of Nanodiamond Sizes on the Efficiency of the Quasi-Specular Reflection of Cold Neutrons, **Materials 16** (2023) 703	01.01.2023	Bosak, A.; Dubois, M.; Korobkina, E.; Lychagin, E.; Muzychka, A.; Nekhaev, G.; Nesvizhevsky, V.; Nezvanov, A.; Saerbeck, T.; Schweins, R.; Strelkov, A.; Turlybekuly, K.; Zhernenkov, K.	Optimal sizes of DNDs (~10 nm) are found for quasi-specular reflection of cold neutrons (CNs).
Enhanced directional extraction of very cold neutrons using a diamond nanoparticle powder reflector, **Rev. Sci. Instr. 93** (2022) 123302	01.12.2002	Chernyavsky, S.M.; Dubois, M.; Korobkina, E.; Lychagin, E.V.; Muzychka, A.Y.; Nekhaev, G.V.; Nesvizhevsky, V.V.; Nezvanov, A.Y.; Strelkov, A.V.; Zhernenkov, K.N.	A major gain (a factor of ~10) in the directed flux of VCNs due the use of DND reflectors is demonstrated experimentally.
Why very cold neutrons could be useful for neutron-antineutron oscillation searches, **J. Neutr. Res. 24** (2002) 223	05.01.2023	Nesvizhevsky, V.	A concrete scheme for using DND reflectors at ESS for the enhancement of VCN fluxes (a factor of ~10) is proposed.
Effect of Particle Sizes on the Efficiency of Fluorinated Nanodiamond Neutron Reflectors, **Nanomaterials 11** (2021) 3067	14.11.2021	Aleksenskii, A.; Bleuel, M.; Bosak, A.; Chumakova, A.; Dideikin, A.; Dubois, M.; Korobkina, E.; Lychagin, E.; Muzychka, A.; Nekhaev, G.; Nesvizhevsky, V.; Nezvanov, A.; Schweins, R.; Shvidchenko, A.; Strelkov, A.; Turlybekuly, K.; Vul, A.; Zhernenkov, K.	Optimal sizes of F-DNDs (~5 nm) are found for diffusive reflection of very cold neutrons (VCNs).
Clustering of Diamond Nanoparticles, Fluorination and Efficiency of Slow Neutron Reflectors, **Nanomaterials 11** (2021) 1945	28.06.2021	Aleksenskii, A.; Bleuel, M.; Bosak, A.; Chumakova, A.; Dideikin, A.; Dubois, M.; Korobkina, E.; Lychagin, E.; Muzychka, A.; Nekhaev, G.; Nesvizhevsky, V.; Nezvanov, A.; Schweins, R.; Shvidchenko, A.; Strelkov, A.; Turlybekuly, K.; Vul, A.; Zhernenkov, K.	De-agglomeration of F-DNDs improves the efficiency of F-DND reflectors.
Fluorination of Diamond Nanoparticles in Slow Neutron Reflectors Does Not Destroy Their Crystalline Cores and Clustering While Decreasing Neutron Losses, **Materials 13** (2020) 3337	27.07.2020	Bosak, A.; Dideikin, A.; Dubois, M.; Ivankov, O.; Lychagin, E.; Muzychka, A.; Nekhaev, G.; Nesvizhevsky, V.; Nezvanov, A.; Schweins, R.; Strelkov, A.; Vul', A.; Zhernenkov, K.	We confirmed that fluorination does not affect the scattering properties of F-DNDs while largely reduces neutron losses.

This project has received funding from the European Union's Horizon 2020 research and innovation programme under grant agreement No. 871072.

A Multitechnique Study of Fluorinated Nanodiamonds for Low-Energy Neutron Physics Applications, **J. Phys. Chem. C 124** (2020) 14229	02.07.2020	Herraiz, M.; Batisse, N.; Dubois, M.; Nesvizhevsky, V.V.; Cavallari, C.; Brunelli, M.; Pischedda, V.; Radescu, S.	We performed a detailed characterization of standard fluorinated nanodiamonds (F-DNDs) as the first step towards the design of optimized F-DNDs.

This project has received funding from the European Union's Horizon 2020 research and innovation programme under grant agreement No. 871072.

Development of reflectors based on fluorinated detonation nanodiamonds (F-DNDs) for very cold neutrons (VCNs) and cold neutrons (CNs)
Publication of results on VCN transmission through novel VCN moderator materials

We performed several series of measurements with samples of designed fluorinated detonation nanodiamonds (F-DNDs), using small-angle neutron scattering (SANS) at D17 and PF1B instruments at ILL, small-angle X-ray scattering (SAXS) at ID10 instrument at ESRF, neutron activation analysis (NAA) at PF1B instrument at ILL, neutron prompt-gamma analysis (NPGA) at PF1B instrument at ILL, neutron diffraction (ND) at PF1B instrument at ILL, quasi-specular neutron reflection (QSNR) at D17 and PF1B instruments at ILL, storage of very cold neutrons (VCNs) at PF2 instrument at ILL, etc.

For these studies, we used standard ILL instruments also developed a new spectrometer/diffractometer option, which can be temporarily installed at PF1B instrument (in the framework of standard ILL user activities). It includes the following options: ND, SANS, NAA, NPGA, QSNR. In contrast to any alternative existing facility, at PF1B instrument, ND can be measured in the full VCN and CN energy range of interest to almost all scattering angles; all mentioned methods of measurements could be applied to the same sample with the same neutron beam, thus reducing various systematics effects.

Analysis of these results has allowed us to develop the optimum designed F-DND powders with parameters which can be “tuned” for any particular application.

Direct beneficiaries of these developments are ILL and ESS (also practically all other neutron centers where the technology of F-DND reflectors for slow neutrons can be used). UCA and UNIMIB contributed to the development of the method and are indirect beneficiaries because they will be needed for any further implementation of the method.

The main highlights are the following:

We published 7 articles including high-impact journals, in particular Nanomaterials (h=5.7), Journal of Physical Chemistry C (h=4.2), Materials (h=3.7), Review of Scientific Instruments (h=1.8), Journal of Neutron Research (h=0.26). This article completely describe all the performed works within the project.

1. We performed a detailed characterization of standard fluorinated nanodiamonds (F-DNDs) as the first step towards the design of optimized F-DNDs [M. Herraiz, et al, *A multitechnique study of fluorinated nanodiamonds for low-energy neutron physics applications*, **J. Phys. Chem. C 124** (2020) 14229].

Here and further on, many non-neutron and neutron techniques are always used for every sample. In the figures below, ^{19}F – 19^{th} isotope of fluorine; MAS NMR – magic angle spinning nuclear magnetic resonance; PTFE – a calibration Teflon sample; CF_2, $CF_{0.018}$ and $CF_{0.079}$ – samples with different C and F ratio; sp^2 and sp^3 – different types of hybridization of carbon; FTIR – Fourier Transform InfraRed spectroscopy; PDF and XRS – neutron and X-ray diffraction methods.

This project has received funding from the European Union’s Horizon 2020 research and innovation programme under grant agreement No. 871072.

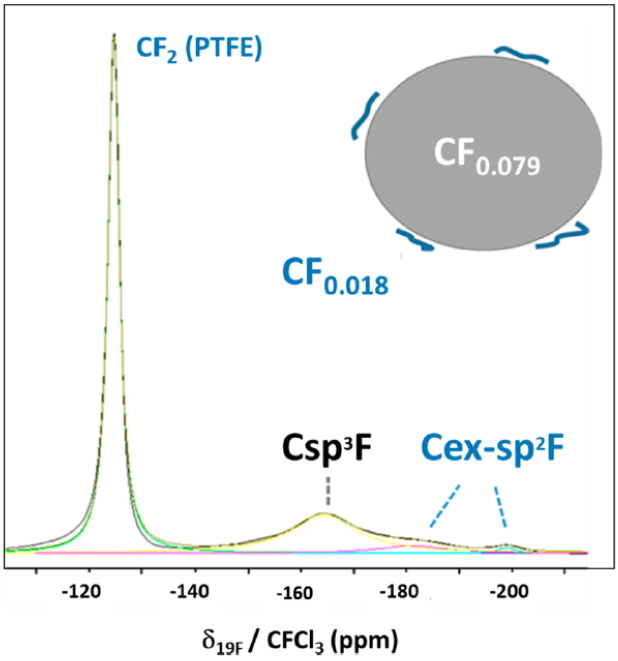

Figure 1. ^{19}F MAS NMR (30 kHz) of fluorinated NDs mixed with PTFE reference for quantification purposes.

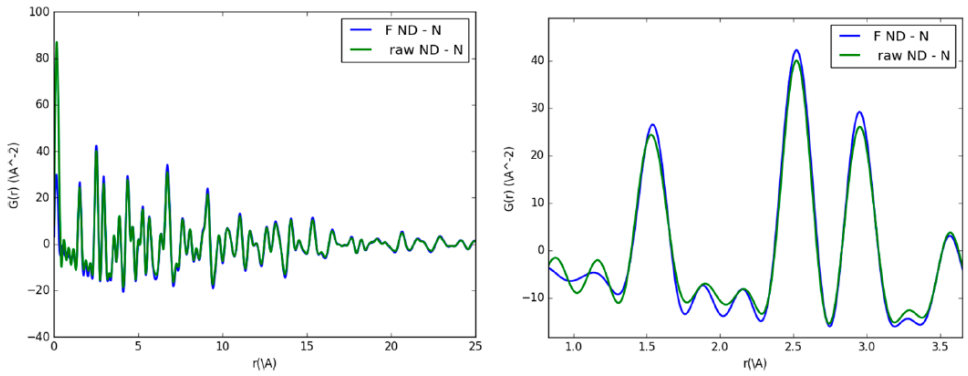

Figure 2. Experimental neutron PDFs of raw and fluorinated NDs plotted up to r = 25 Å (left panel) and magnifications, collected at the diffractometer D4C (ILL, Grenoble), using an incident neutron wavelength λ = 0.4989 Å and Q_{max} = 23.5 Å^{-1}.

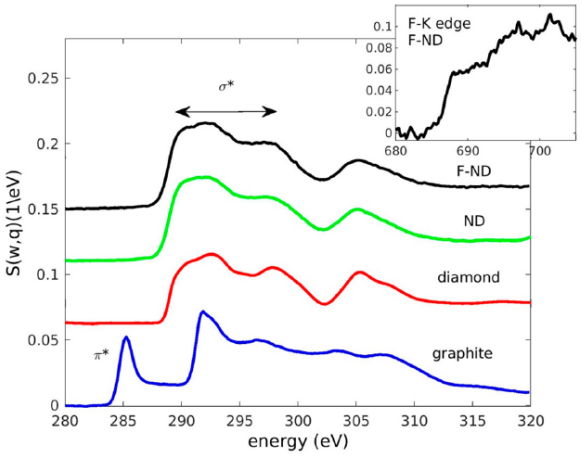

Figure 3. XRS spectra at the carbon K edge of F-NDs, NDs, graphite, and diamond powder. Graphite and diamond powders are reported as an example of pure C-sp^2 and C-sp^3 hybridization (data published in ref 29). In the inset, XRS spectra at the F−K edge for F-NDs.

This project has received funding from the European Union's Horizon 2020 research and innovation programme under grant agreement No. 871072.

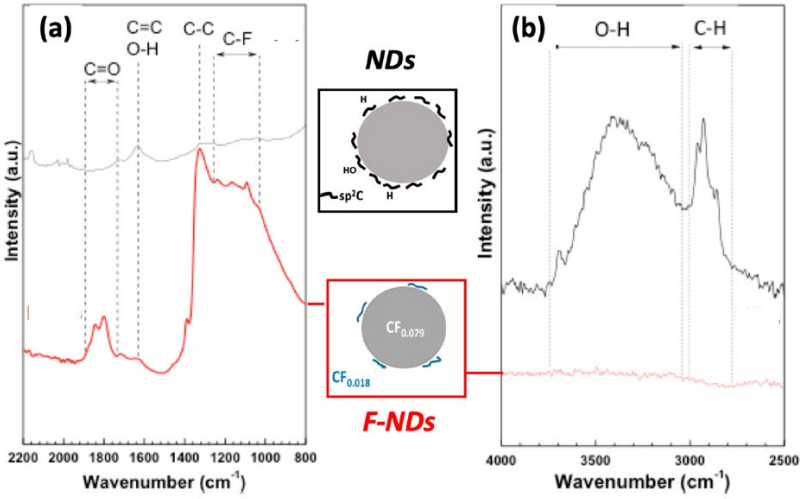

Figure 4. FTIR spectra (ATR mode) of raw and fluorinated NDs.

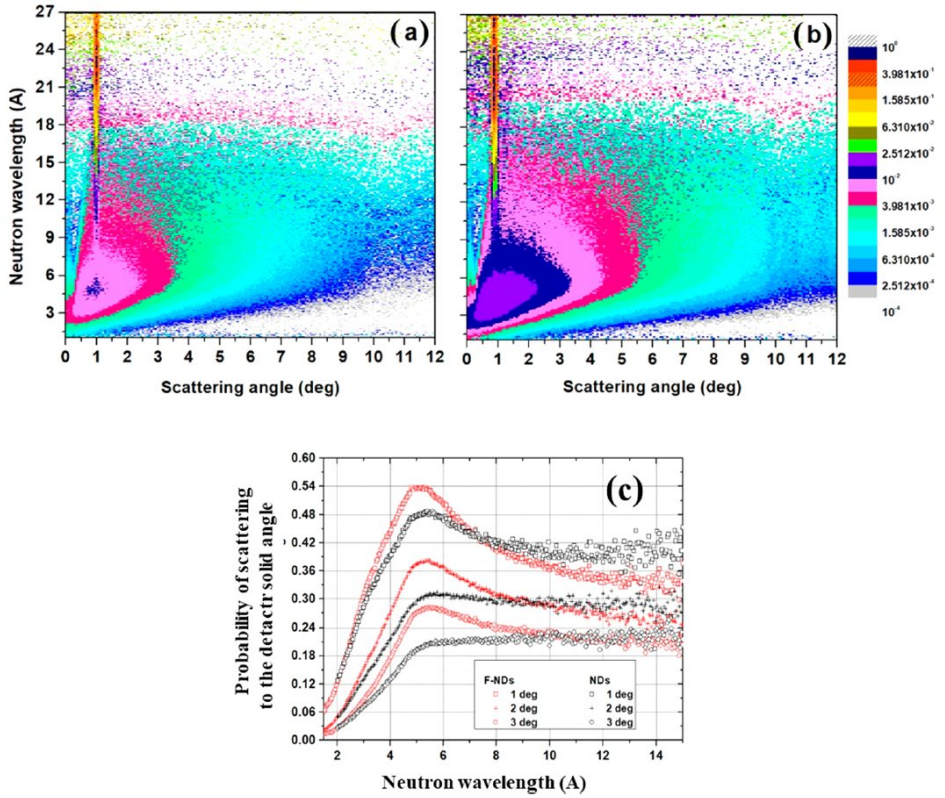

Figure 5. An example of quasi-specular scattering data measured with NDs (a) and F-NDs (b) samples at D17 instrument at ILL. Different intensities/colors (in the inset on right) indicate a relative number of neutrons, as a function of scattering angle (*X*-axis, in degrees) and neutron wavelength (*Y*-axis, in Å). The neutron incidence angle equals 1°. (c) Differential probability of neutron scattering, measured as a function of neutron wavelength (Å), from F-NDs (in red) and NDs (in black) to the angular acceptance of D17 detector in the geometry indicated in Figure SI1. We integrated data over the whole range of scattering angles, and normalized them to total incident intensity. The incidence angle is 1°, 2°, and 3°, respectively, as indicated in the inset.

2. We confirmed that fluorination does not affect the scattering properties of F-DNDs while largely reduces neutron losses [A. Bosak, et al, Fluorination of Diamond Nanoparticles in Slow Neutron Reflectors Does Not Destroy Their Crystalline Cores and Clustering While Decreasing Neutron Losses, Materials 13 (2020) 3337].

In the figures below, TEM – transmission electron microscopy; SEM – scanning electron microscopy.

This project has received funding from the European Union's Horizon 2020 research and innovation programme under grant agreement No. 871072.

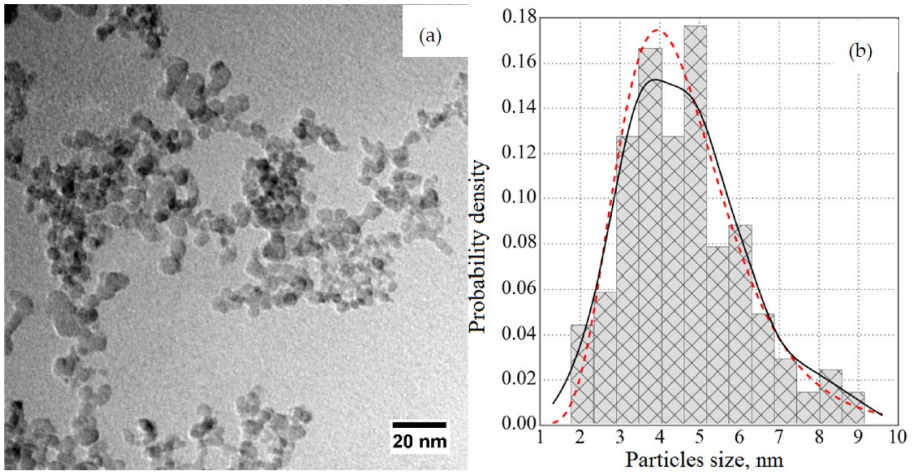

Figure 1. (**a**) A TEM image of the fluorinated nanodiamonds (F-DND) sample, (**b**) a corresponding diameter distribution of the DNDs. The red dashed line corresponds to the lognormal distribution. The black solid line indicates a data fitting.

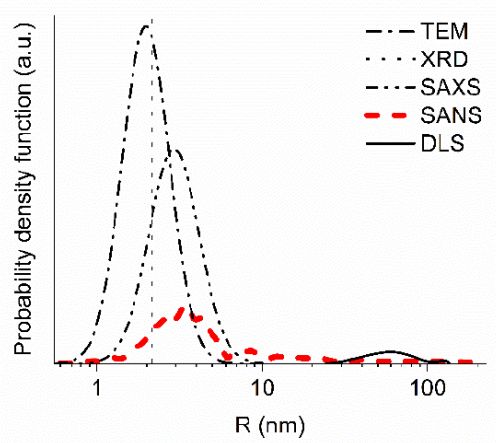

Figure 2. The probability density as a function of radius (nm) evaluated using neutron small-angle scattering (SANS) (red thick dashed line), X-ray small-angle scattering (SAXS) (black thin dash-double-dotted line), TEM (black thin dash-dotted line), and dynamic light scattering (DLS) (black thin solid line). The vertical black dotted line indicates a mean radius measured with XRD. All measurements are performed with F-DND samples, except for SAXS, which is performed with a DND sample. The details of the different measurements are given below in the text.

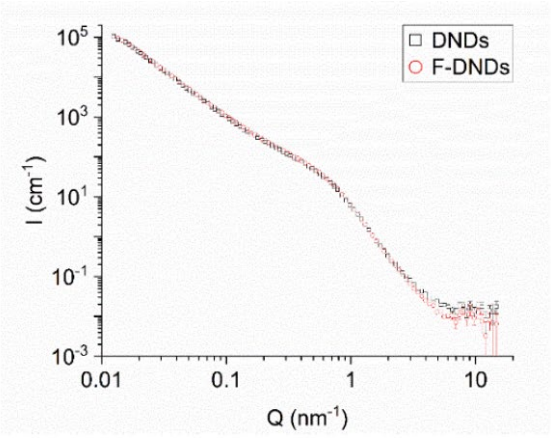

Figure 3. Measured intensity I (cm^{-1}) of scattered neutrons as a function of the transferred momentum Q (cm^{-1}) for DND and F-DND samples shown with black squares and red circles, respectively. For the convenience of comparing the results, the data are normalized to the equal sample mass.

This project has received funding from the European Union's Horizon 2020 research and innovation programme under grant agreement No. 871072.

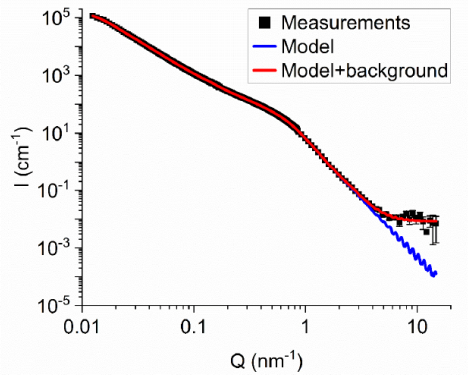

Figure 4. Comparison of measured and simulated intensity I (cm^{-1}) of neutron scattered as a function of the transferred momentum Q (cm^{-1}) for the F-DND sample. Black squares denote the experimental data. The thin blue line shows the results of the simulation within the model of discrete-size diamond nanospheres, and the thick red line contains in addition the background intensity of $9{\cdot}10^{-3}$ nm^{-1}.

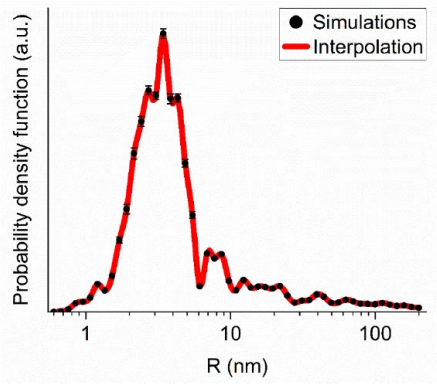

Figure 5. The probability density as a function of radius (in nm) evaluated within the model of discrete-size diamond nanospheres for the F-DND sample. Red circles show the simulation results. The red solid line interpolates the simulation results.

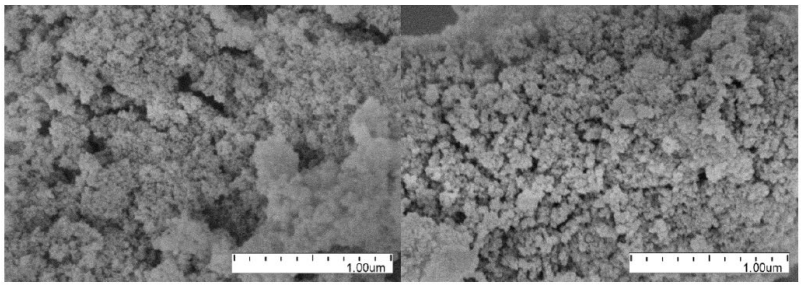

Figure 6. Examples of SEM images of DNDs (**on left**) and F-DNDs (**on right**).

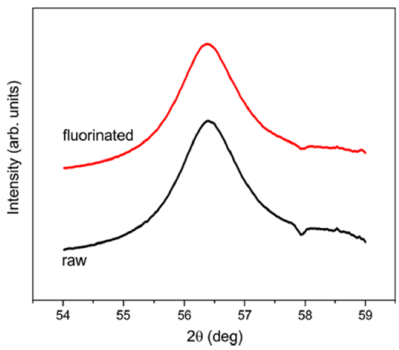

Figure 7. Powder diffraction for DND (black lower line) and F-DND (red upper line, shifted in intensity for better visibility) samples in the proximity of a 422 Debye-Scherrer ring. Full width at half maximum (FWHM) from the Lorentz line shape fit were evaluated to 1.343 ± 0.018 and 1.354 ± 0.022 for DND and F-DND samples, respectively, therefore coinciding. The mean size of DND cores is 4.3 nm.

This project has received funding from the European Union's Horizon 2020 research and innovation programme under grant agreement No. 871072.

3. De-agglomeration of F-DNDs improves the efficiency of F-DND reflectors [A. Aleksenskii, et al, Clustering of Diamond Nanoparticles, Fluorination and Efficiency of Slow Neutron Reflectors, Nanomaterials 11 (2021) 1945];

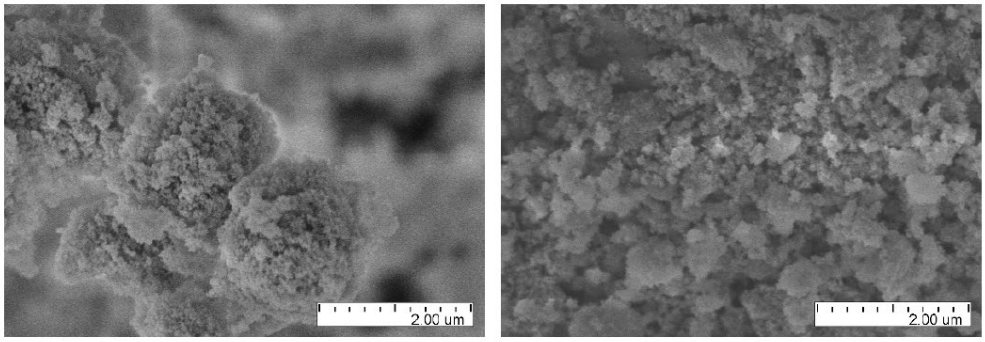

(c) (d)

Figure 1. Examples of SEM images: (**a**,**b**) DF-DNDs; (**c**,**d**) F-DNDs.

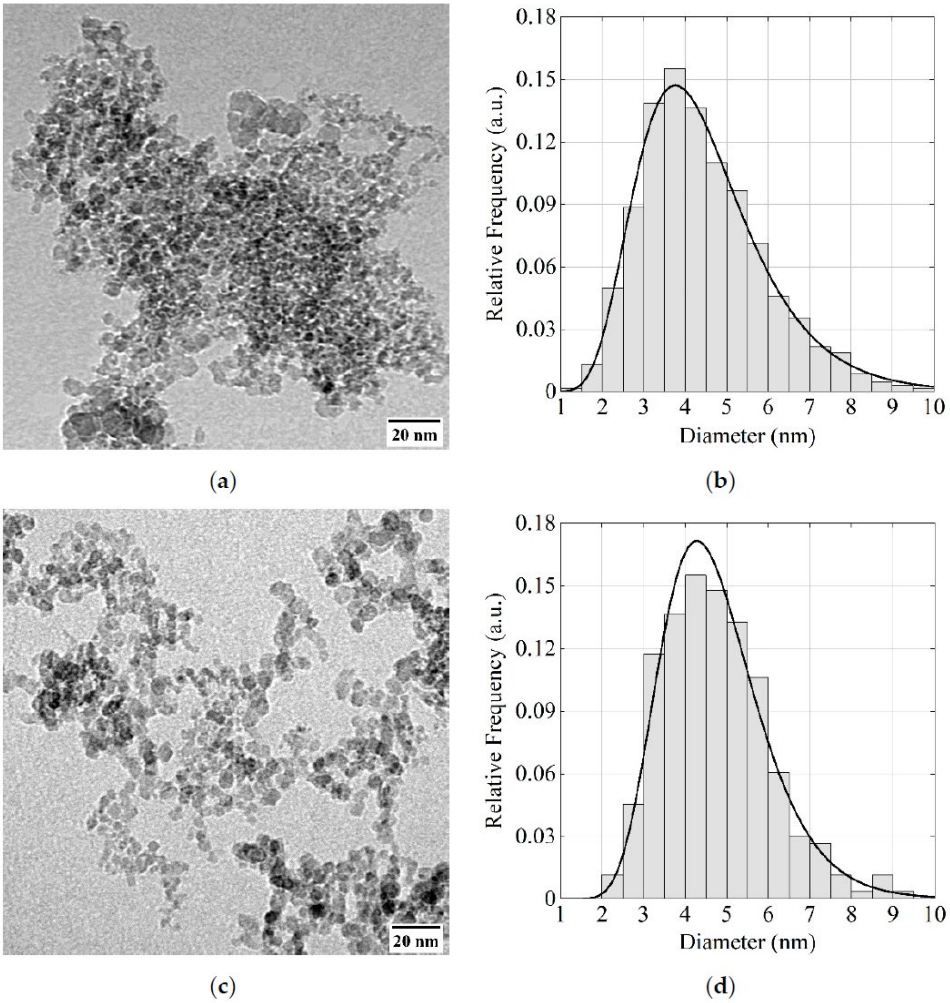

(a) (b)

(c) (d)

Figure 2. (**a**,**c**) TEM images of the F-DND and DF-DND samples; (**b**,**d**) respective diameter distributions of the DNDs. Black solid lines correspond to the lognormal distribution.

This project has received funding from the European Union's Horizon 2020 research and innovation programme under grant agreement No. 871072.

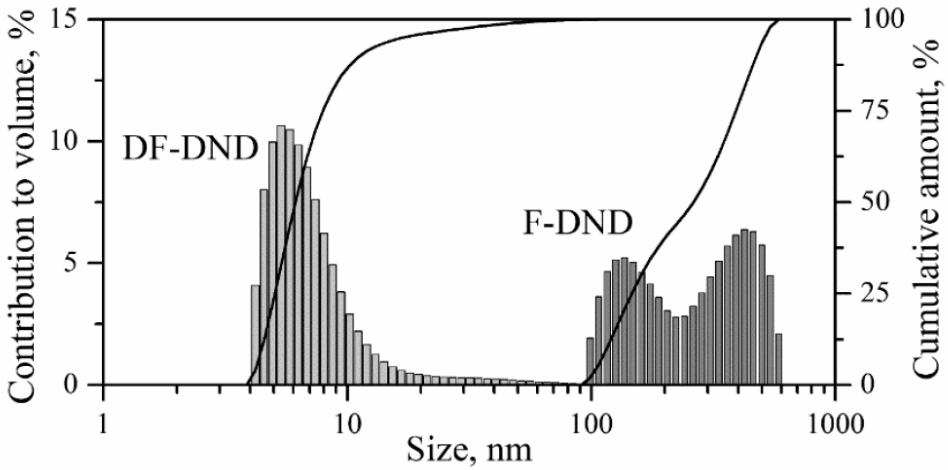

Figure 3. Size distributions in F-DNDs and DF-DNDs in ethanol measured by the DLS method.

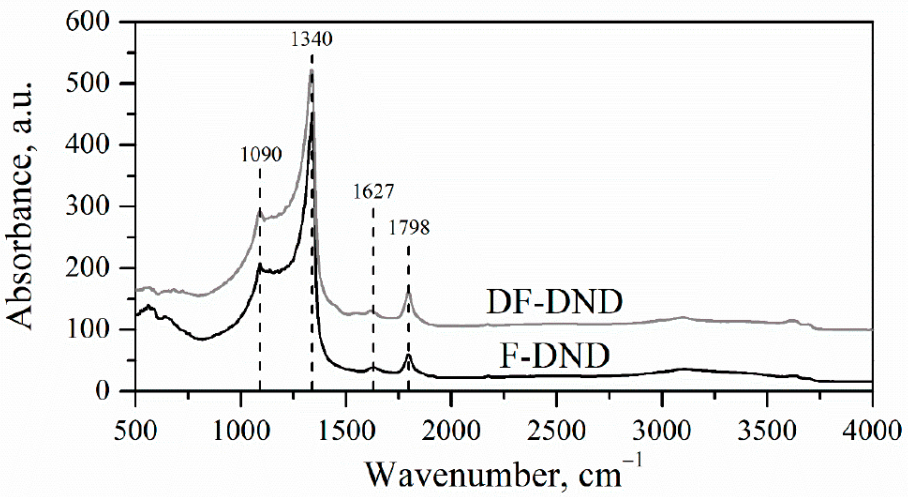

Figure 4. IR spectra of F-DNDs and DF-DNDs.

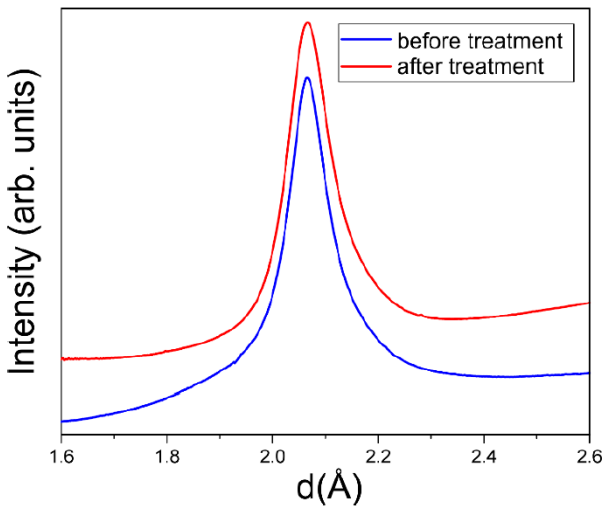

Figure 5. Profile of 111 diamond diffraction peak before and after the deagglomeration treatment. Graphs are shifted along the vertical axis for the visibility.

This project has received funding from the European Union's Horizon 2020 research and innovation programme under grant agreement No. 871072.

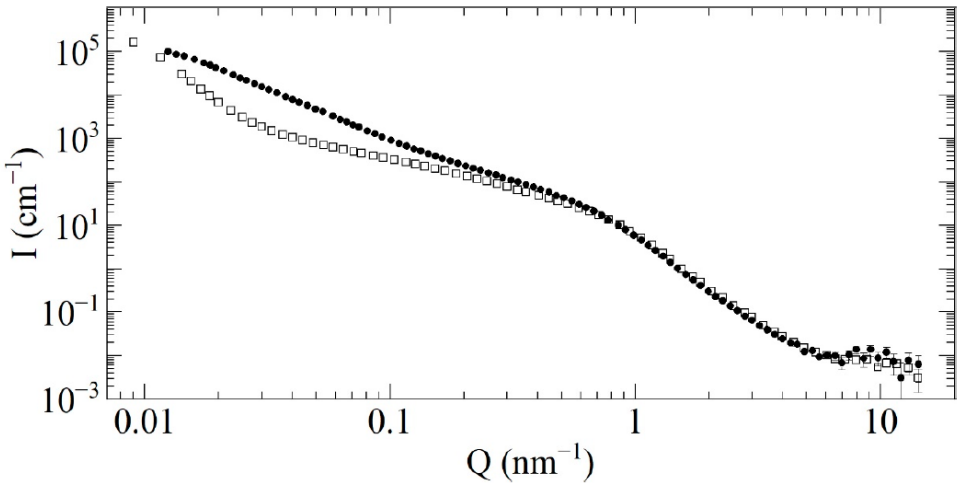

Figure 6. The intensity I (cm^{-1}) of scattering versus the neutron-transferred momentum Q (cm^{-1}) for the F-DNDs (solid circles) and DF-DNDs (open squares). Both curves are normalized to the equal sample density of 0.19 g/cm^3.

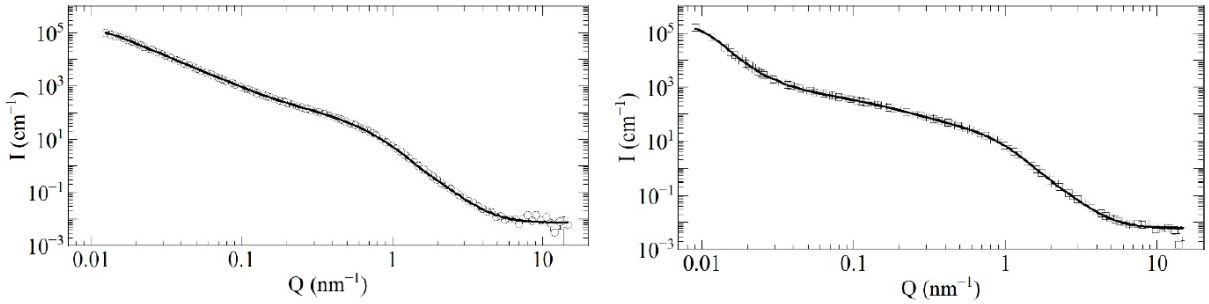

Figure 7. Comparison of measured (open circles and squares) and simulated (solid lines) scattering intensity I (cm^{-1}) versus the neutron-transferred momentum Q (nm^{-1}): (**a**) F-DND; (**b**) DF-DND samples.

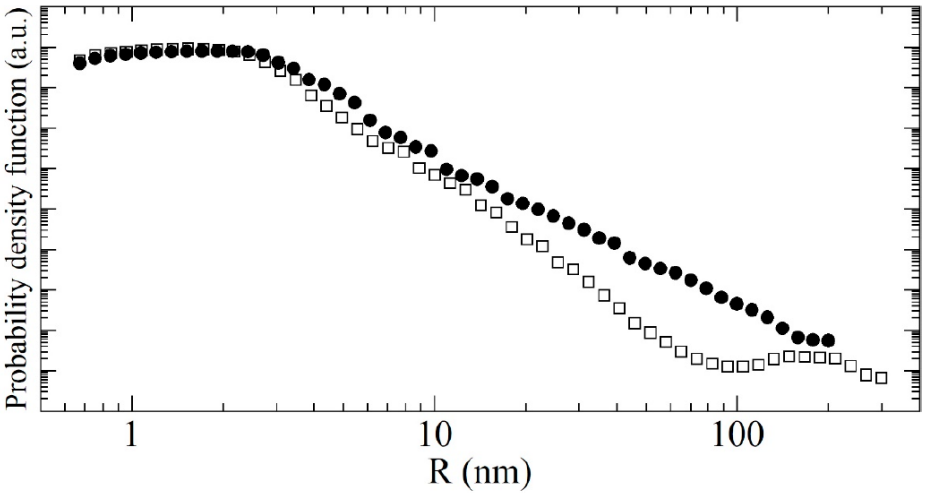

Figure 8. The probability density versus radius (in nm) calculated with the discrete-sized diamond nanospheres model for the F-DNDs (solid circles) and DF-DNDs (open squares). Points correspond to the results of calculation.

This project has received funding from the European Union's Horizon 2020 research and innovation programme under grant agreement No. 871072.

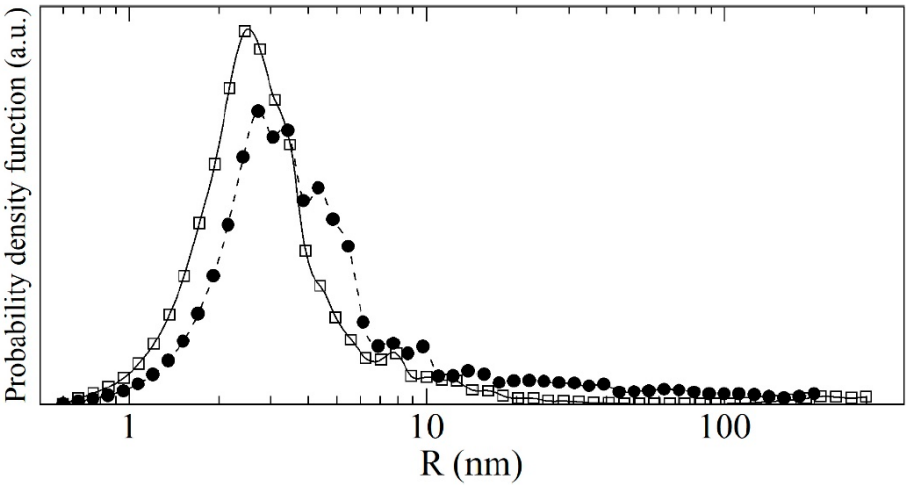

Figure 9. The log-linear volume distribution of scatterers evaluated using the discrete-sized diamond nanospheres model for the F-DNDs (solid circles) and DF-DNDs (open squares). Solid (DF-DNDs) and dashed (F-DNDs) lines interpolate the calculated results.

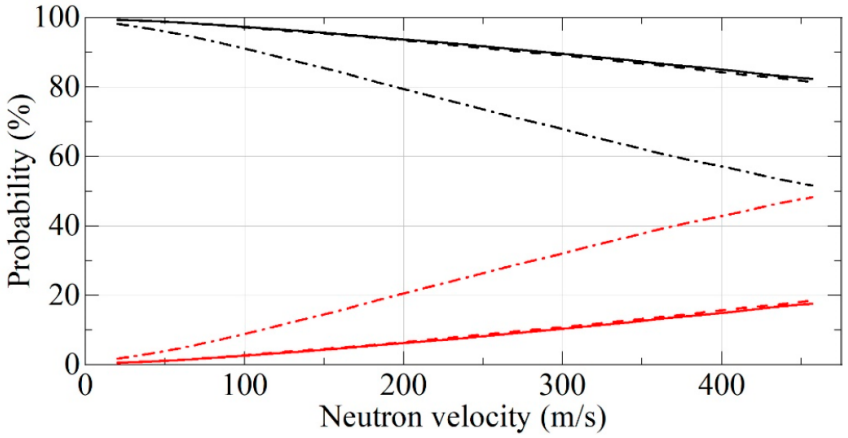

Figure 10. The probability of neutron reflection (black lines) and absorption (red lines) for F-DNDs (dashed lines) and DF-DNDs (solid lines) and DNDs (dash-dotted lines) versus neutron velocity. The incident neutrons are isotropic, the powder density is 0.19 g/cm^3, and the powder thickness is infinite.

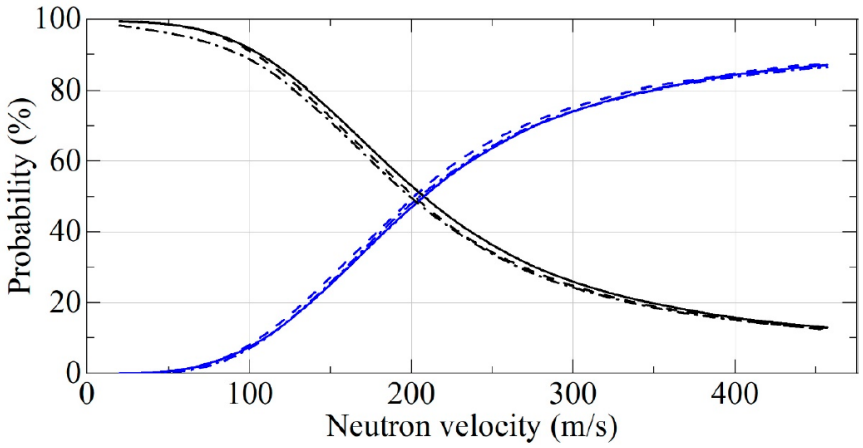

Figure 11. The probability of neutron reflection (black lines) and transmission (blue lines) for F-DNDs (dashed lines) and DF-DNDs (solid lines) and DNDs (dash-dotted lines) versus neutron velocity. The probability of neutron absorption is below 1% for F-DNDs and DF-DNDs at any velocity and 1–5% for DNDs. The incident neutrons are isotropic, the powder density is 0.19 g/cm^3, and the powder layer thickness is 3 cm.

This project has received funding from the European Union's Horizon 2020 research and innovation programme under grant agreement No. 871072.

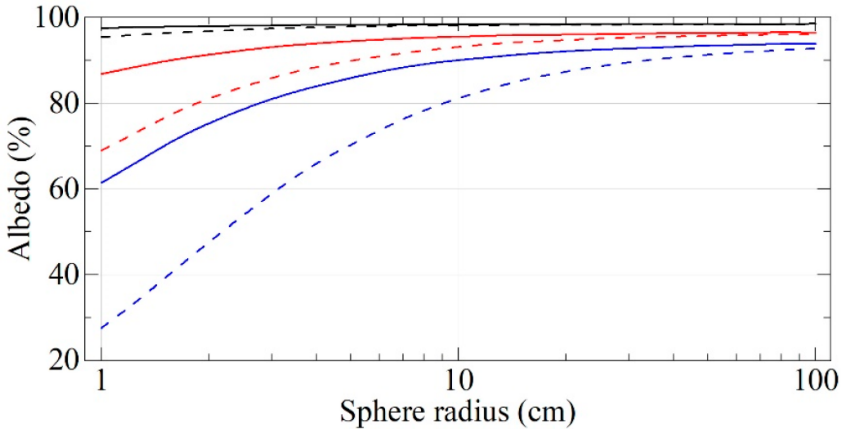

Figure 12. Neutron albedo for the velocities of 50 m/s (black lines), 100 m/s (red lines), and 150 m/s (blue lines) for F-DNDs (dashed lines) and DF-DNDs (solid lines) versus the cavity radius. The incident neutrons are isotropic, the powder thickness is infinite, and densities of F-DNDs and DF-DNDs are equal to 0.19 and 0.56 g/cm^3, respectively.

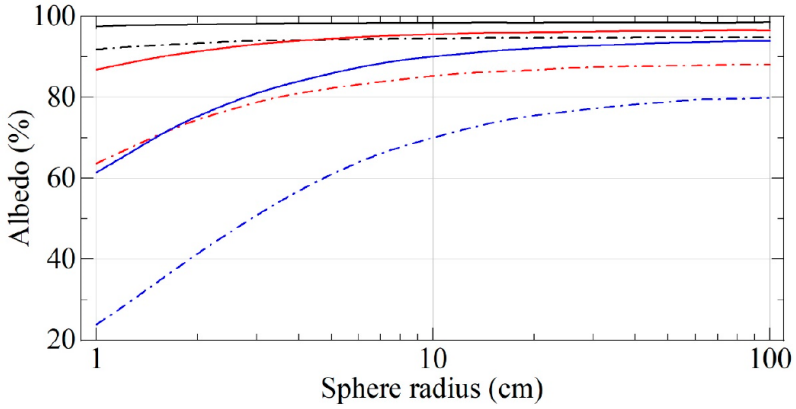

Figure 13. Neutron albedo for the velocities of 50 m/s (black lines), 100 m/s (red lines), and 150 m/s (blue lines) for DF-DNDs (solid lines) and DNDs (dash-dotted lines) versus the cavity radius. The incident neutrons are isotropic; the powder thickness is infinite. DF-DNDs density is equal to 0.56 g/cm^3. The DNDs density is the same as it is in Figure 12 and equal to 0.19 g/cm^3.

4. Optimal sizes of F-DNDs (~5 nm) are found for diffusive reflection of very cold neutrons (VCNs) [A. Aleksenskii, et al, Effect of Particle Sizes on the Efficiency of Fluorinated Nanodiamond Neutron Reflectors, Nanomaterials 11 (2021) 3067];

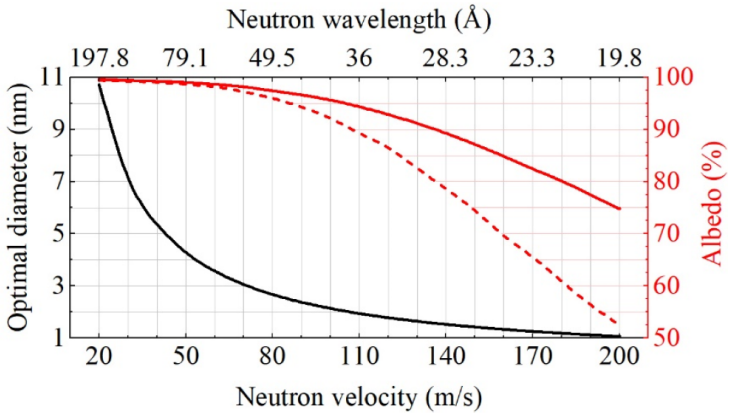

Figure 1. Optimal diameters of diamond nanospheres (black line) as a function of VCN velocity/wavelength. Solid red line shows the corresponding calculated VCN albedo for the optimal diameters of diamond nanospheres. Dashed red line stands for the VCN albedo from real DF-DNDs (see ref. [46]). Neutrons are only absorbed by carbon atoms.

This project has received funding from the European Union's Horizon 2020 research and innovation programme under grant agreement No. 871072.

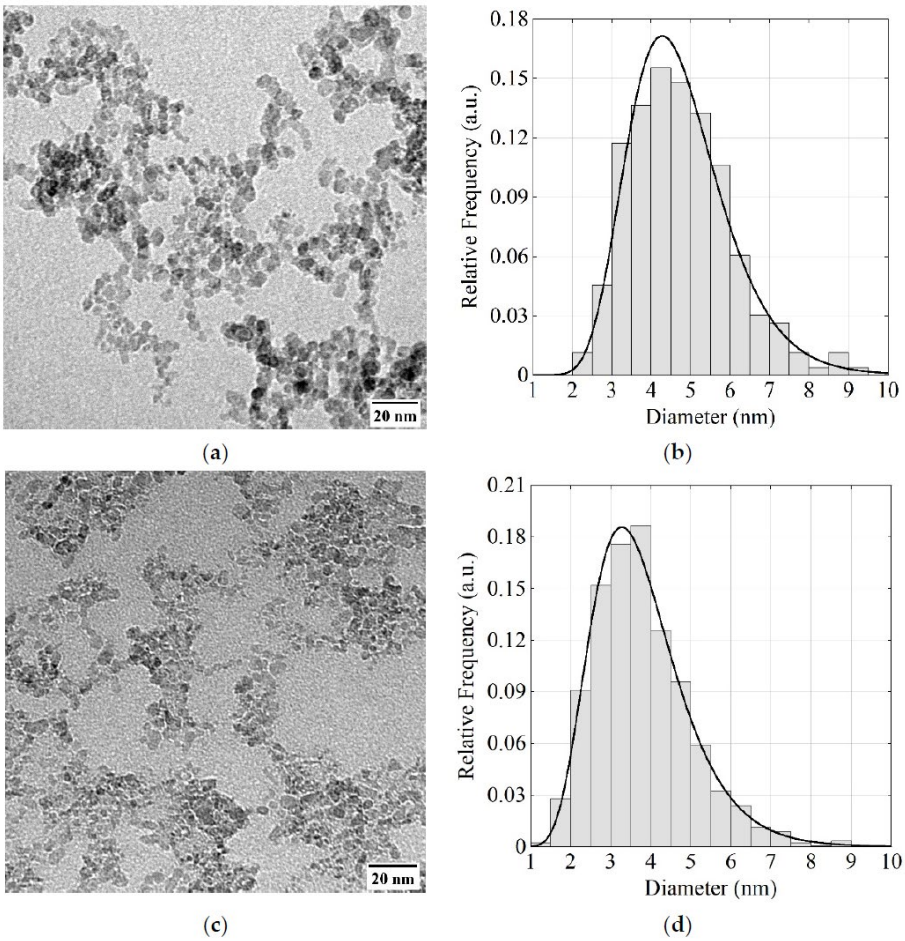

Figure 2. (**a**,**c**) Examples of TEM images of the DF-DND and S-DND samples; (**b**,**d**) size distributions for DF-DNDs and S-DNDs evaluated using all TEM images available.

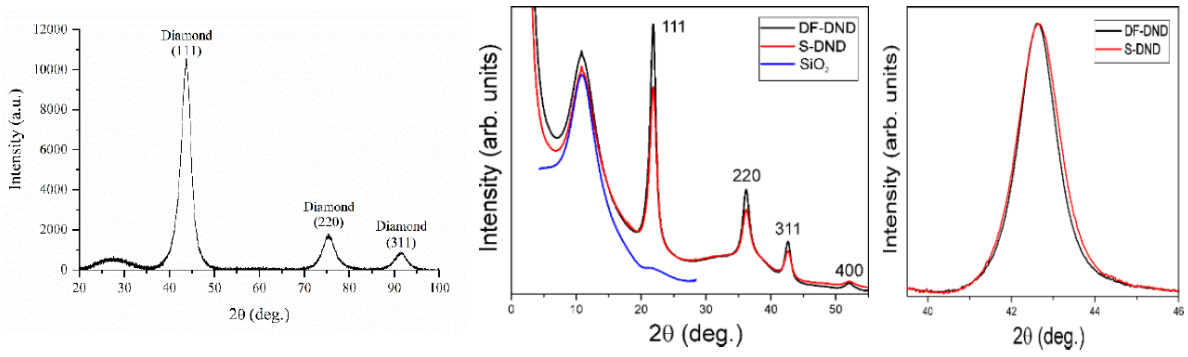

Figure 3. X-ray diffraction patterns: (**a**) S-DNDs at Rigaku SmartLab III; background is subtracted. (**b**) ESRF ID28 data for DF-DNDs and S-DNDs composed of three sets corresponding to three positions of the 2D detector; empty capillary scattering is shown. (**c**) Close-up of the 311 peak with the subtracted background and peak rescaling.

This project has received funding from the European Union's Horizon 2020 research and innovation programme under grant agreement No. 871072.

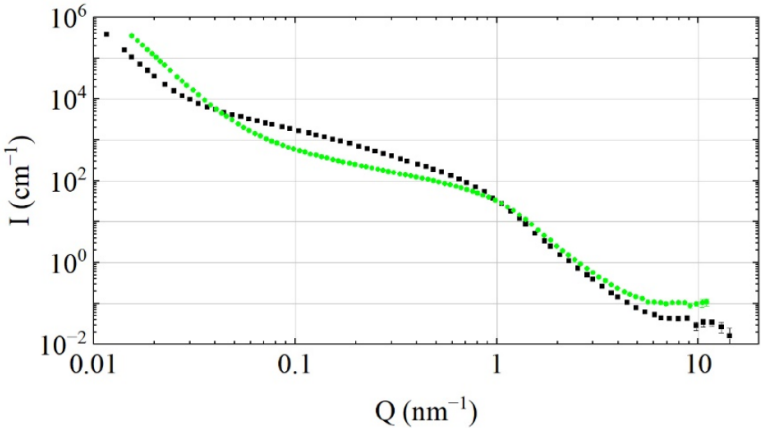

Figure 4. Intensity I (nm^{-1}) of neutron scattering versus transferred momentum Q (nm^{-1}) for DF-DNDs (black squares) and S-DNDs (green circles). To compare only the effect of particle sizes, and not powder density, both curves are normalized to the sample density of 1 g/cm^3. SANS characterization was performed with YuMO, D11, and NGB30 instruments, and their neutron wavelengths and ranges of transferred momenta (Q) were equal to 0.7–5.0 Å and 7×10^{-2} nm^{-1} < Q < 10^1 nm^{-1}; 6 Å and 10^{-2} nm^{-1} < Q < 10^0 nm^{-1}; and 6 Å and 3.4×10^{-2} nm^{-1} < Q < 1.2×10^0 nm^{-1}, respectively. The Q-ranges used for the summary plot for the S-DNDs are as follows: 1.55×10^{-2} nm^{-1}–8.53×10^{-1} nm^{-1} from D11 and 8.53×10^{-1} nm^{-1}–1.10×10^0 nm^{-1} from YuMO; for the DF-DNDs, they are as follows: 9.03×10^{-3} nm^{-1}–1.55×10^{-2} nm^{-1} and 7.57×10^{-2} nm^{-1}–9.85×10^{-2} nm^{-1} from NGB30, 1.55×10^{-2} nm^{-1}–7.57×10^{-2} nm^{-1} from D11, and 9.85×10^{-1} nm^{-1}–1.47×10^0 nm^{-1} from YuMO.

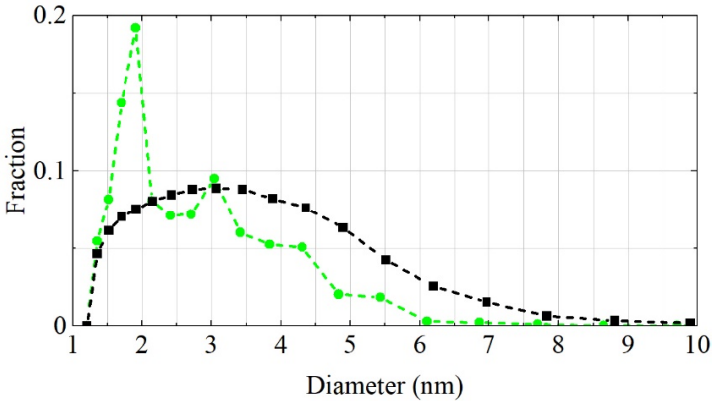

Figure 5. Size distribution of scatterers evaluated using MDDNS for S-DNDs (green circles) and DF-DNDs (black squares). Points correspond to the results of calculation.

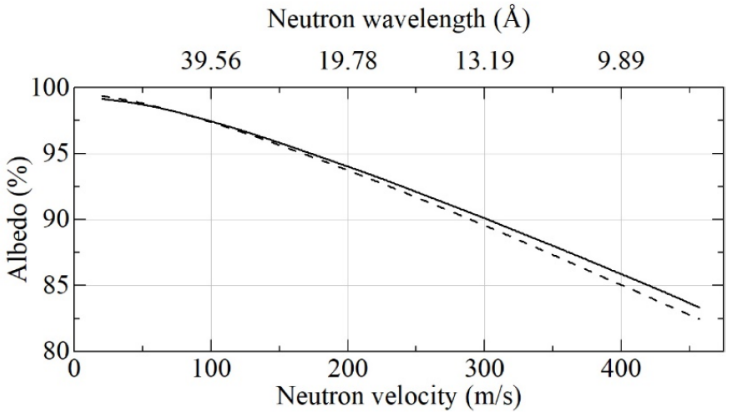

Figure 6. Neutron albedo for the flat semi-infinite media of DF-DNDs (dashed lines) and S-DNDs (solid lines) versus neutron velocity and wavelength.

This project has received funding from the European Union's Horizon 2020 research and innovation programme under grant agreement No. 871072.

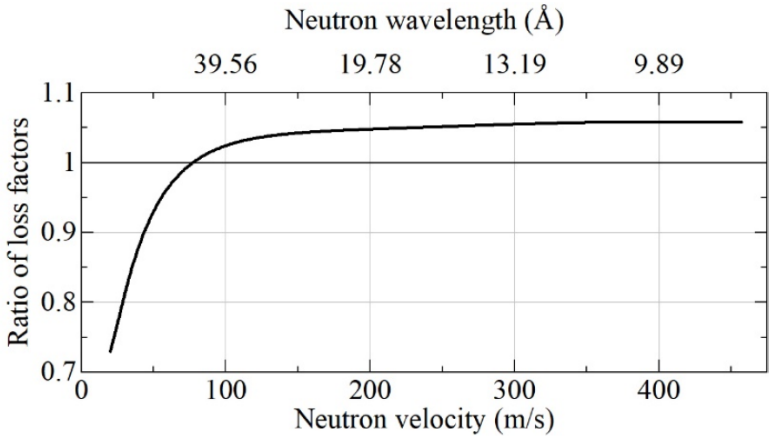

Figure 7. Ratio of loss factors η_(DF-DNDs)/η_(S-DNDs) at reflection from flat semi-infinite media of DF-DNDs and S-DNDs as a function of neutron velocity. The respective neutron albedo is shown in Figure 6.

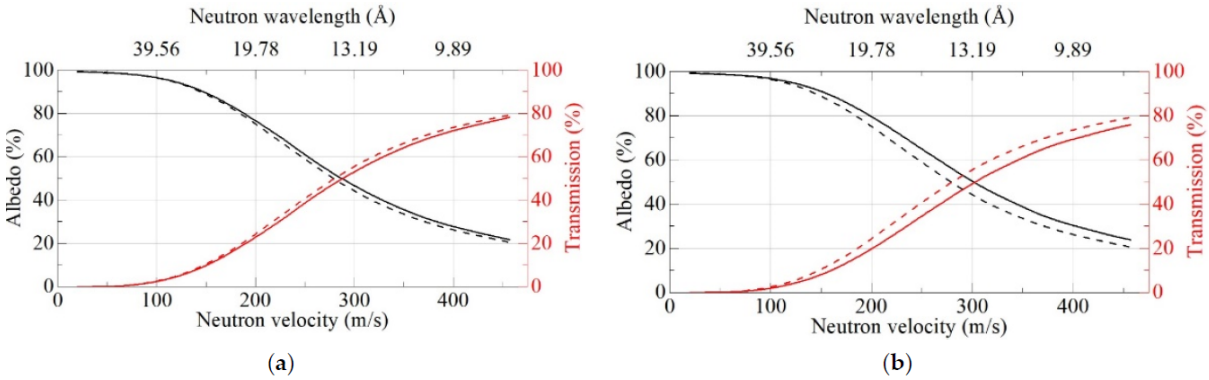

Figure 8. Neutron albedo (black lines) and transmission (red lines) for a flat layer of DF-DNDs (dashed lines) and S-DNDs (solid lines) versus neutron velocity [m/s]. (**a**) The layer thickness is 3 cm and the powder density is 0.56 g/cm^3 for both samples; (**b**) the layer thickness is 3 cm and the powder density is 0.56 g/cm^3 for DF-DNDs, and it is 0.67 g/cm^3 for S-DNDs.

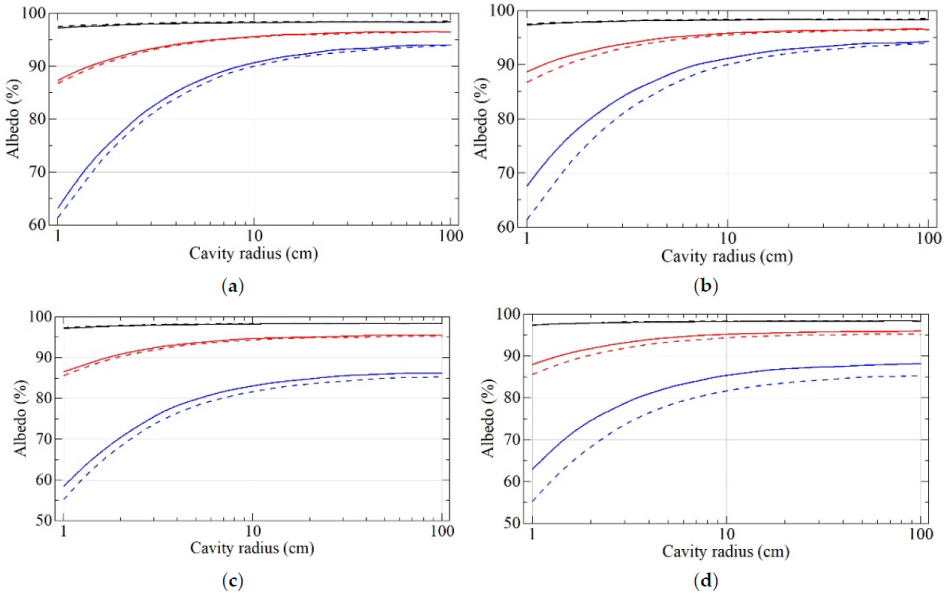

Figure 9. Neutron albedo for the velocities of 50 m/s (black lines), 100 m/s (red lines), and 150 m/s (blue lines) for S-DNDs (solid lines) and DF-DNDs (dashed lines) versus the cavity radius. (**a**) A powder layer of infinite thickness; the density is 0.56 g/cm^3 for both samples. (**b**) A powder layer of infinite thickness; the density is 0.56 g/cm^3 for DF-DNDs, and it is 0.67 g/cm^3 for S-DNDs. (**c**) A powder layer with the thickness of 3 cm; the density is 0.56 g/cm^3 for both samples. (**d**) A powder layer with the thickness of 3 cm; the density is 0.56 g/cm^3 for DF-DNDs, and it is 0.67 g/cm^3 for S-DNDs.

This project has received funding from the European Union's Horizon 2020 research and innovation programme under grant agreement No. 871072.

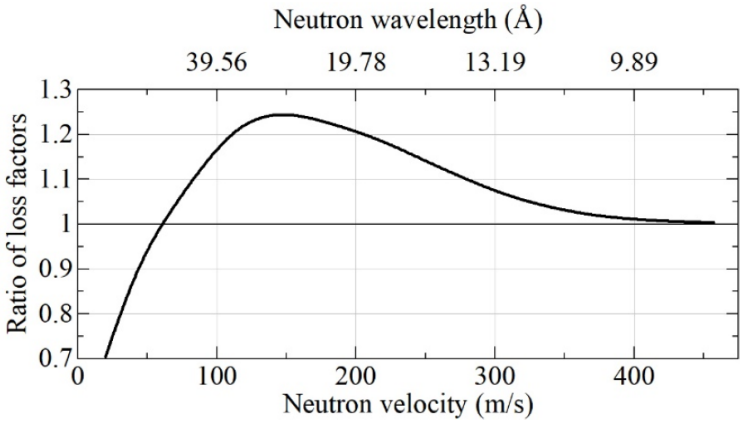

Figure 10. Ratio of loss factors $\eta_{DF-DNDs}/\eta_{S-DNDs}$ at reflection from the wall of a spherical cavity with a radius of 5 cm and a wall thickness of 3 cm for realistic powder densities of 0.56 g/cm^3 for DF-DNDs and 0.67 g/cm^3 for S-DNDs.

5. A concrete scheme for using DND reflectors at ESS for the enhancement of VCN fluxes (a factor of ~10) is proposed [V.V. Nesvizhevsky, Why very cold neutrons could be useful for neutron-antineutron oscillation searches, J. Neutron Res. 24 (2022) 223].

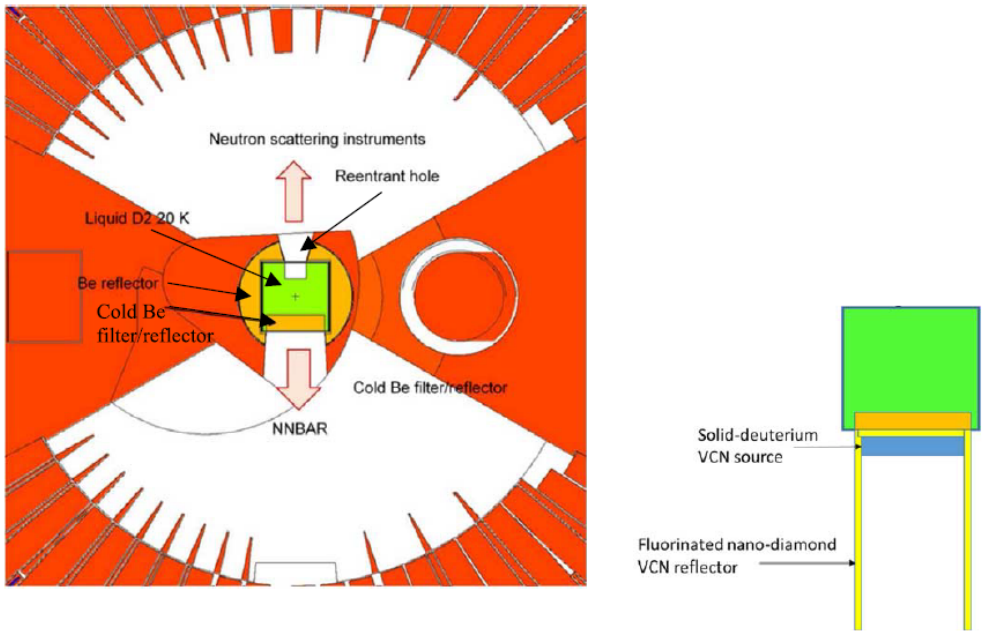

Fig. 1. Figure is taken from "L. Zanini et al., Very Cold and Ultra Cold Neutron Sources for ESS, these proceedings". At left, the current design for the implementation of a large-volume liquid-deuterium source of CN. The green coloring indicates regions of 20 K. The downward facing arrow at bottom illustrates CN passing through a Be filter (orange) and feeding a $n-\overline{n}$ experiment. A dedicated solid-deuterium VCN converter with an F-DND reflector could be added to this design, as is shown below.

6. A major gain (a factor of ~10) in the directed flux of VCNs due the use of DND reflectors is demonstrated experimentally [Chernyavsky, S.M., et al, Enhanced directional extraction of very cold neutrons using a diamond nanoparticle powder reflector, Rev. Sci. Instr. 93 (2022) 123302].

This project has received funding from the European Union's Horizon 2020 research and innovation programme under grant agreement No. 871072.

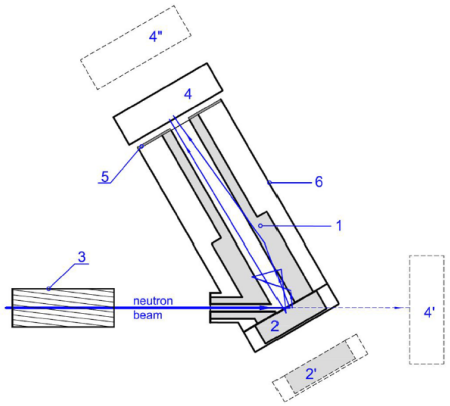

FIG. 1. Schematic layout of the experimental setup: (1)—a cylindrical tube made of reflector; (2)—a reflector in the disk shape; (2′)—the disk position when measuring the incident beam flux; (3)—a rotating velocity selector with screw slits; (4)—a position-sensitive detector (PSD) for measuring the flux of escaping neutrons; (4′)—the PSD position when measuring the incident beam flux; (4″)—the PSD position when measuring the angular distribution of escaping neutrons; (5)—a Cd-diaphragm; and (6)—an evacuated volume.

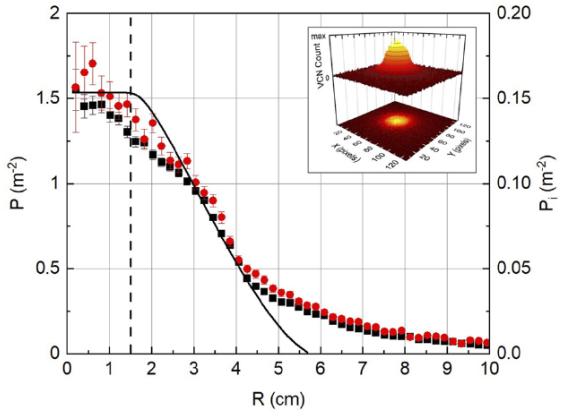

FIG. 2. The left axis and dots correspond to the radial dependence of the specific probability of VCN detection, $P(R, v)$ (see the text for the definition). Round dots correspond to a neutron velocity of ~57 m/s, square dots to ~75 m/s. Right axis and solid line indicate the specific probability $P_i(R, v)$ of VCN detection calculated for the homogeneous isotropic source. The vertical dashed line stands for the reflector cavity and the Cd diaphragm radii. The insert shows a map of the PSD counts by pixels (the pixel size is ~2 mm) in measurements with a velocity of ~75 m/s.

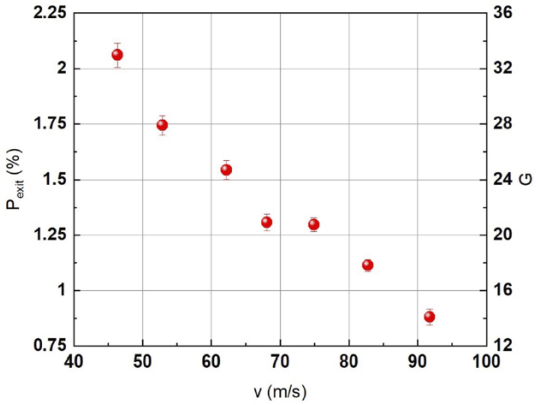

FIG. 4. Left axis: a fraction P_{exit}, in percent, of VCN flux escaping through the diaphragm to VCN flux incident into the cavity as a function of VCN velocity. Right axis: gain factor G in the escaping flux relative to the flux that would pass through the diaphragm from a homogeneous isotropic source with the intensity of the incidence beam located at the cavity bottom.

This project has received funding from the European Union's Horizon 2020 research and innovation programme under grant agreement No. 871072.

7. Optimal sizes of DNDs (~10 nm) are found for quasi-specular reflection of cold neutrons (CNs). [A. Bosak, et al, Effect of Nanodiamond Sizes on the Efficiency of the Quasi-Specular Reflection of Cold Neutrons, Materials 16 (2023) 703].

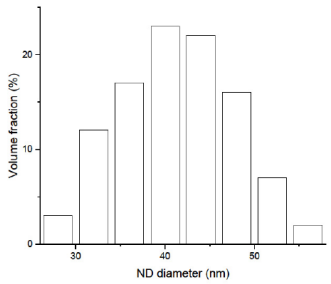

Figure 1. Diameter distribution of ND in the SCD powder measured by Ferran using a Beckman Coulter laser diffraction particle size analyzer. Note that the sensitivity of the method sharply decreases for small NDs (below ~30 nm), and the method should not be used in this range.

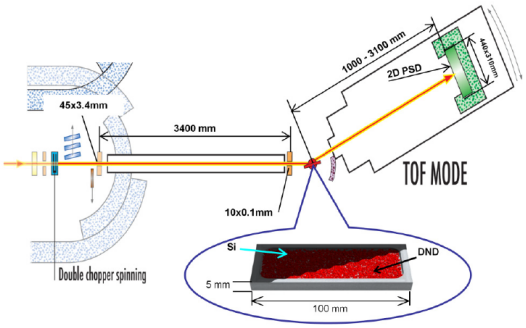

Figure 2. Top view scheme of measurements of the QSR of neutrons from the powder of NDs. The circled magnification shows a sample of ND powder (red) in a sample container. The double chopper periodically interrupts the incident neutron beam, thus providing a pulsed neutron spectrum for time-of-flight measurements. Various devices in front of the sample provide background suppression, neutron transport and neutron beam collimation. A position-sensitive ^{3}He detector (2D PSD) is behind the sample. The arrow illustrates a neutron quasi-specularly reflected from the sample.

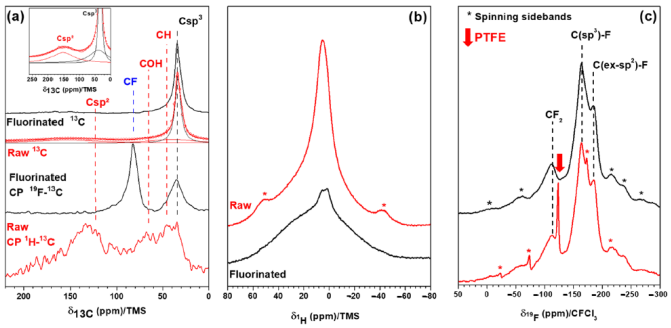

Figure 3. (**a**) ^{13}C MAS (10 kHz) spectra of raw and fluorinated SCD (^{1}H→^{13}C and ^{19}F→^{13}C CP were also used for raw and fluorinated samples); (**b**) ^{1}H MAS (14 kHz); (**c**) ^{19}F MAS (14 kHz) spectra.

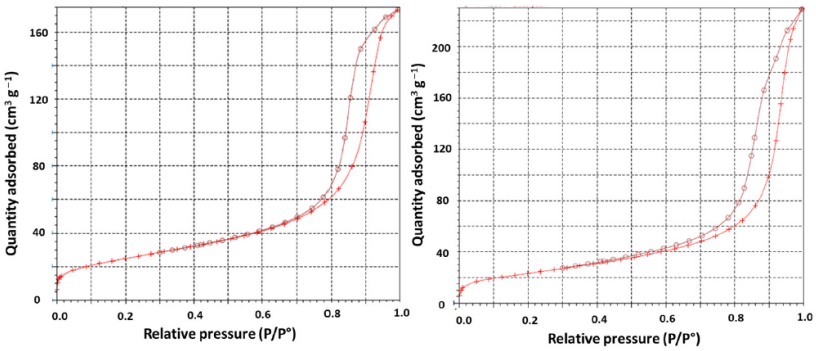

Figure 4. Adsorption and desorption isotherms of SCD (**left**) and F-SCD (**right**).

This project has received funding from the European Union's Horizon 2020 research and innovation programme under grant agreement No. 871072.

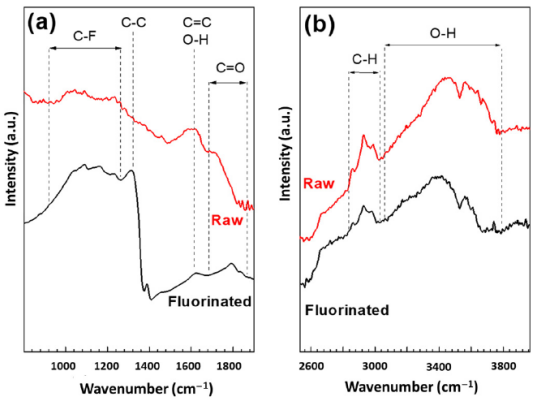

Figure 5. IR spectra of raw and fluorinated SCD in the two ranges of interest (**a**,**b**).

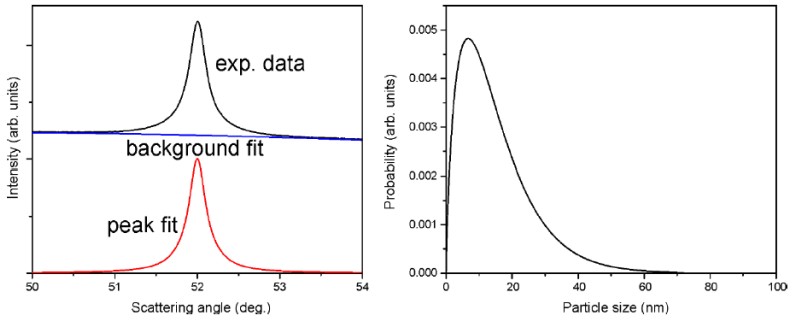

Figure 6. XRD results for the SCD sample. (**Left**): 400 diffraction line shape and its fit. The noise level is comparable to the line thickness. (**Right**): Evaluated ND size distribution function [40].

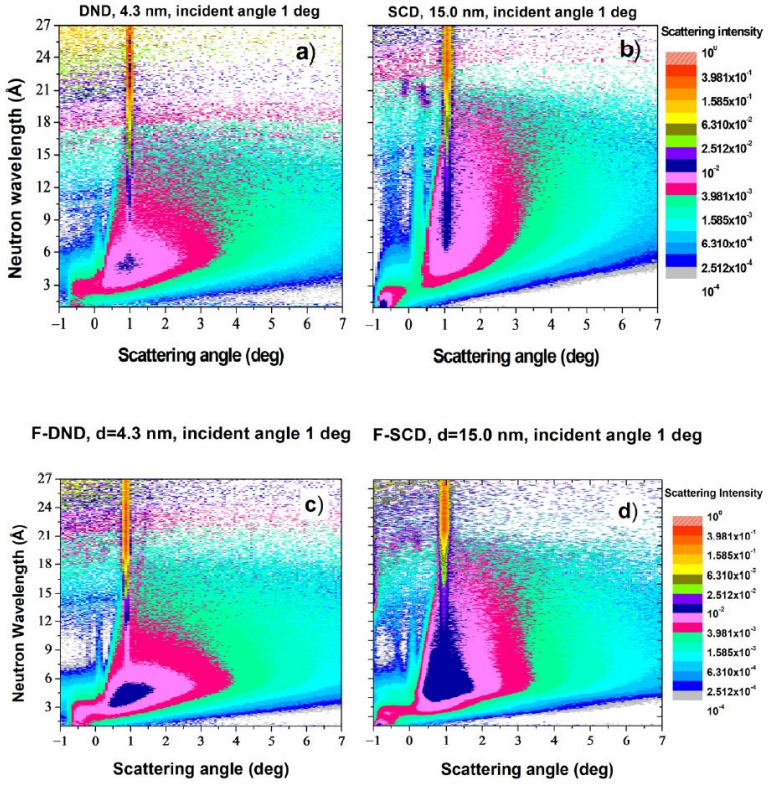

Figure 7. Probability of neutron scattering from the surface of ND samples as a function of the neutron wavelength (vertical axis) and the scattering angle in the direction perpendicular to the plane of the sample (horizontal axis). Different colors are scaled to the proportion of neutrons registered in the detector normalized by the incident beam flux. Samples: (**a**) DND; (**b**) SCD; (**c**) F-DND; (**d**) F-SCD. In all cases, the angle of incidence of the neutron beam onto the sample was 1°.

This project has received funding from the European Union's Horizon 2020 research and innovation programme under grant agreement No. 871072.

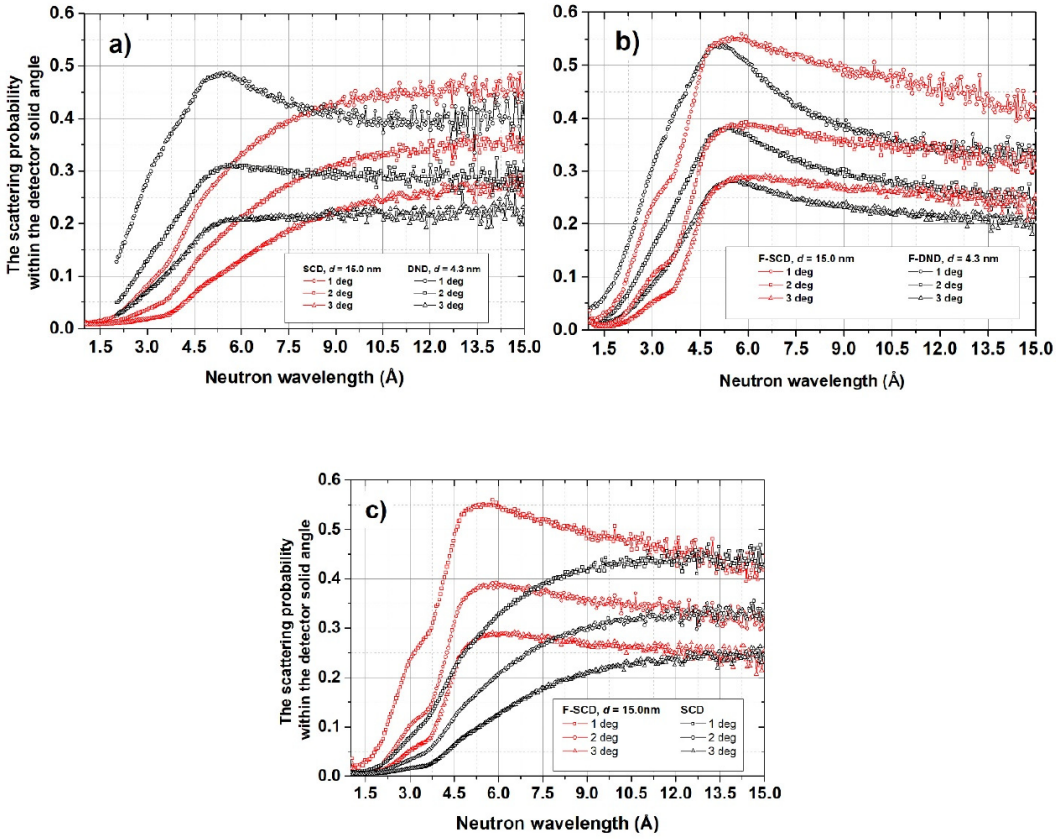

Figure 8. Neutron scattering probability as a function of neutron wavelength (horizontal axis) within the D17 detector acceptance. (**a**) DND and SCD samples; (**b**) F-DND and F-SCD samples; (**c**) SCD and F-SCD samples. Incident angles 1°, 2° and 3°.

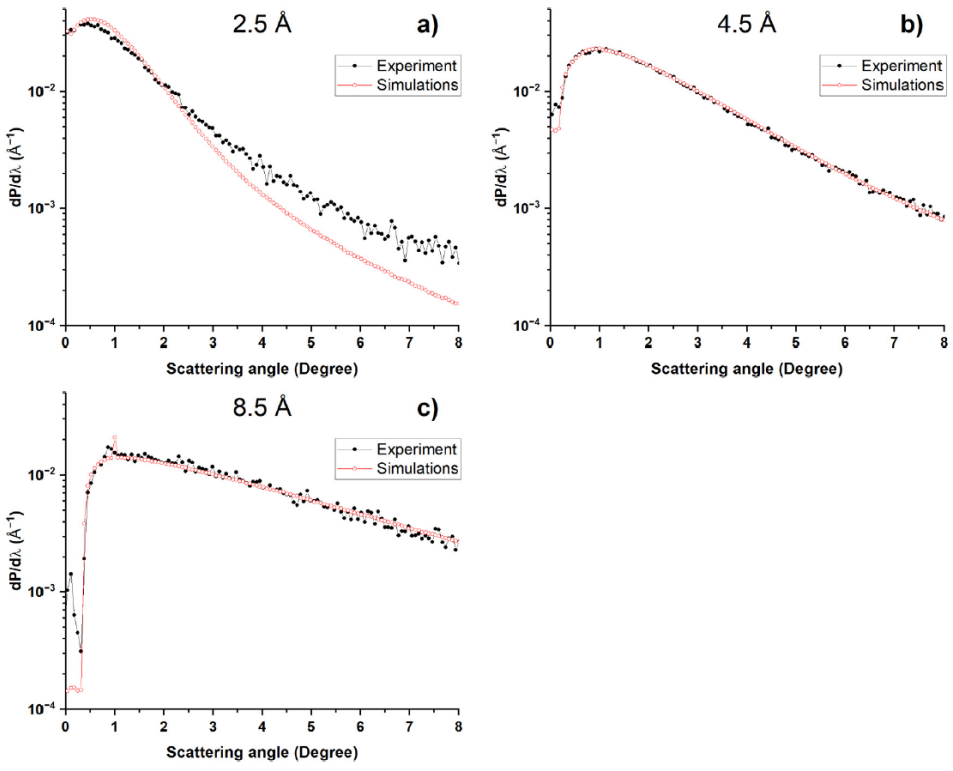

Figure 10. Simulated and measured angular distributions of QSR neutrons for the F-DND sample at three wavelengths: (**a**) 2.5 Å, (**b**) 4.5 Å and (**c**) 8.5 Å. In all cases, the angle of incidence was 1°.

This project has received funding from the European Union's Horizon 2020 research and innovation programme under grant agreement No. 871072.

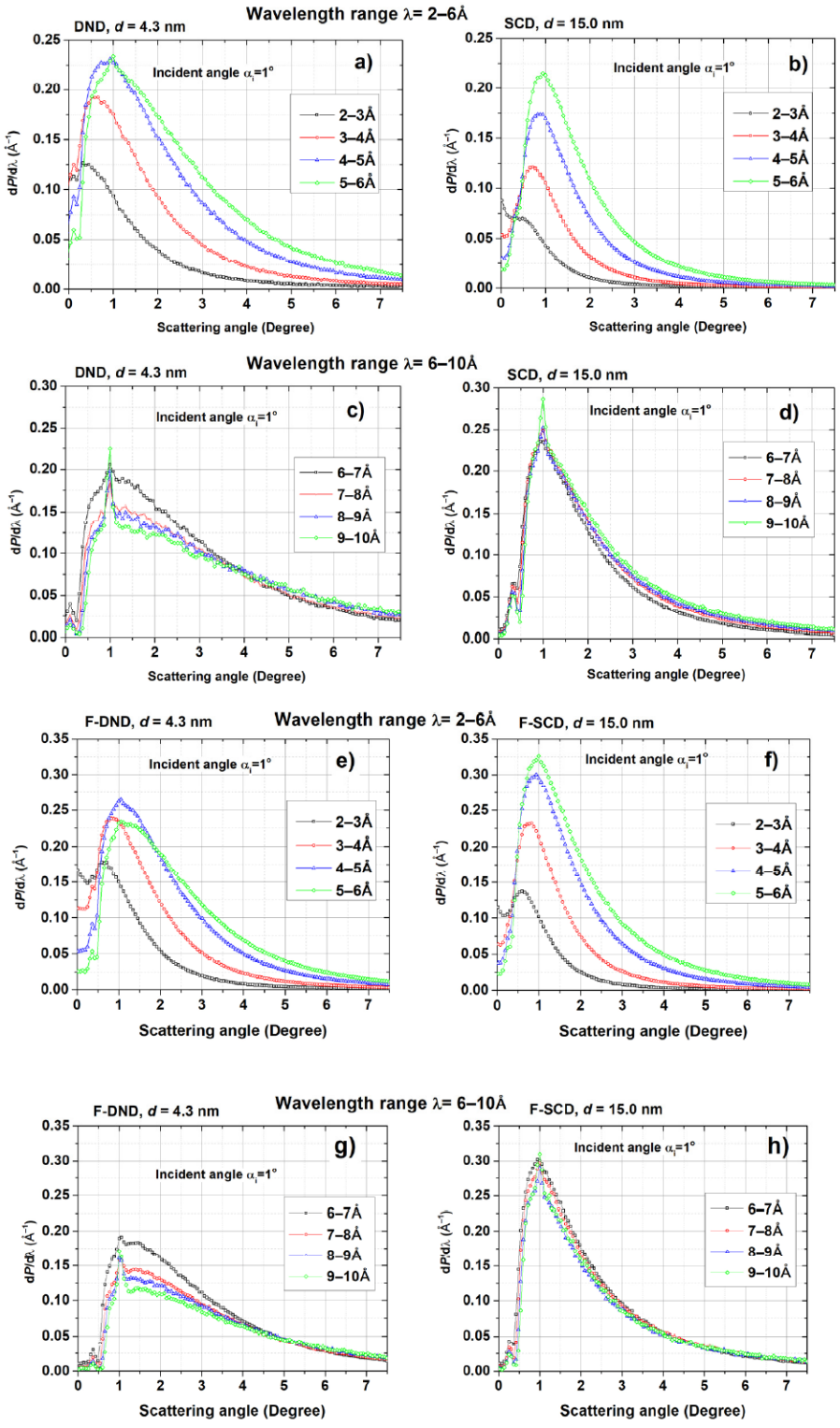

Figure 9. Differential probability of neutron scattering (vertical axis) as a function of the reflectior angle (horizontal axis) within the angular acceptance of the D17 detector. Samples and wavelengtl ranges: (**a**) DND, 2–6 Å; (**b**) SCD, 2–6 Å; (**c**) DND, 6–10 Å; (**d**) SCD, 6–10 Å; (**e**) F-DND, 2–6 Å (**f**) F-SCD, 2–6 Å; (**g**) F-DND, 6–10 Å; (**h**) F-SCD, 6–10 Å. For all cases, the angle of incidence was 1°

This project has received funding from the European Union's Horizon 2020 research and innovation programme under grant agreement No. 871072.

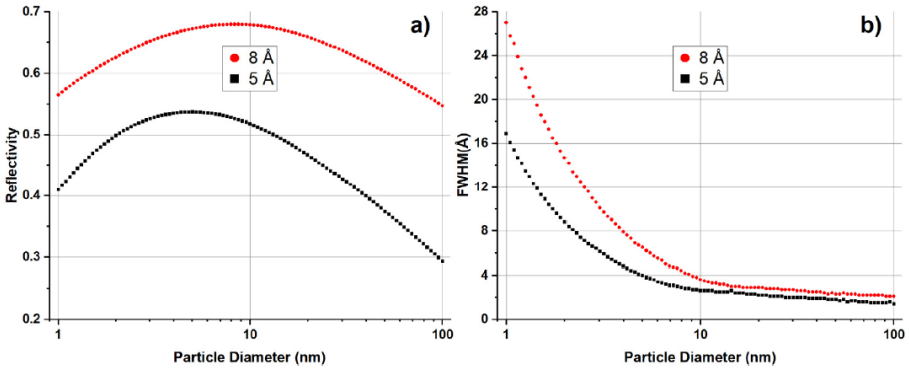

Figure 11. (**a**) Simulated reflectivity and (**b**) angular distribution width as a function of ND diameter. Black squares correspond to calculations for neutrons with wavelengths of 5 Å, and red circles correspond to 8 Å. The angle of incidence was set to 1° in the simulations.

The overlap with other WP or external experts:

The method of quasi-specular reflection of CNs is quite useful for the better extraction of CNs from cold neutron sources (Task 3.1).

Deliverables and Milestones achieved so far:

All deliverables and milestones of this part of the project (F-DND reflectors) are fully achieved.

Status quo:

All tasks of this part of the project (F-DND reflectors) are fully completed.

This project has received funding from the European Union's Horizon 2020 research and innovation programme under grant agreement No. 871072.